

Magnetic ordering and multiferroicity in MnI_2

Xianxin Wu,¹ Yingxiang Cai,² Qing Xie,^{3,1} Hongming Weng,^{1,*} Heng Fan,^{1,†} and Jiangping Hu^{1,4,‡}

¹ Institute of Physics, Chinese Academy of Sciences, Beijing 100190, China

² Department of Physics, Nanchang University, Nanchang 330031, China

³ Department of Physics, Ningbo University, Zhejiang 315211, China

⁴ Department of Physics, Purdue University, West Lafayette, Indiana 47907, USA

(Dated: November 9, 2018)

Density-functional calculations are carried out to investigate incommensurate magnetic structures and ferroelectric polarization in newly discovered multiferroic material MnI_2 . The exchange interactions among local moments on Mn are parameterized by mapping the mean-field Heisenberg model on to total energy difference of several magnetic ordering states. The experimentally observed noncollinear magnetic states are well reproduced by using this model and exchange interaction parameters. The direction of polarization experimentally measured is also consistent with the result derived from the symmetry analysis of the magnetically ordered state. In particular, we find that the inter-plane magnetic exchange coupling is pivotal to the emergence of the spiral magnetic structure. This noncollinear magnetic structure, combined with spin-orbit coupling mainly from I ions, is responsible for the appearance of ferroelectric polarization.

PACS numbers: 75.85.+t, 75.10.Hk, 71.70.Ej, 71.15.Mb

I. INTRODUCTION

Multiferroics, which exhibit magnetic and dielectric order in the same phase, recently have attracted increasing attention^{1,2}. The recent experimental research on multiferroics has shown that ferroelectricity (FE) and magnetism couple so strongly that the electric degree of freedom can be manipulated by an external magnetic field and vice versa³⁻¹². These properties offer unprecedented applications in modern energy-effective electronic data storage technology^{13,14}.

Theoretically, phenomenological models and symmetry analysis have clarified the circumstances where a spiral spin structure can induce an electric polarization^{15,16}. Harris¹⁶ gives a simple method to describe the magnetic ordering and their relationship to ferroelectricity based on lattice, space and time reversal symmetries: the symmetry of the magnetoelectric interaction can determine the direction of spontaneous polarization induced by magnetism.

Several microscopic mechanisms have been proposed to explain the magnetoelectric coupling in multiferroics. One is the well-known Katsura-Nagaosa-Balatsky (KNB) model¹⁷ which is based on the idea that spin currents are induced between the spiral spins and can therefore be considered as electric moments. The second is that the magnetically induced ionic displacements due to Dzyaloshinskii-Moriya (DM) interactions can lead to polarization^{18,19}. The electric cancellation model²⁰ gives a simple but general mechanism to understand the interplay between ferroelectricity and noncollinear magnetism in multiferroics. As a powerful tool to investigate the electronic structure of materials, density functional theory (DFT) has played an important role in the understanding of the collinear-spin type^{21,22} and the spiral magnetic materials LiCu_2O_2 and LiCuVO_4 ²³.

MnI_2 has been investigated primarily due to the interest in magnetic and optical properties²⁴⁻²⁶. However, it has been discovered recently by Kurumaji *et al.*²⁷ that MnI_2 is also a multiferroic material. MnI_2 crystallizes in the CdI_2 type structure with the space group $P\bar{3}m1$ (No.164). The unit

cell contains one formula unit (f.u.) with the manganese ion located at $(0, 0, 0)$ and the iodide ions at $\pm(\frac{1}{3}, \frac{2}{3}, u)$, where $u = 0.245 \pm 0.002$, $a = 4.146 \text{ \AA}$ and $c = 6.829 \text{ \AA}$ ²⁴. Magnetic properties are dominated by Mn^{2+} ion with $S = \frac{5}{2}$. Sato *et al.*²⁵ observed three successive phase transitions at 3.95 K (T_{N1}), 3.8 K (T_{N2}) and 3.45 K (T_{N3}). As temperature decreases, the Bragg reflection at $\mathbf{q}_{im}(q_1, q_2, q_3) \sim (0.1025, 0.1025, 0.5)$ appears at T_{N1} . When the temperature is further decreased, the reflection position begins to move slightly out of the (hhl) plane towards the $(h0l)$ plane. Finally at T_{N3} it jumps to $\mathbf{q}_{it} \sim (0.181, 0, 0.439)$, in which we notice that q_1 is not equal to q_2 . Below T_{N3} , the proper screw magnetic structure is realized, which induces FE polarization about $84 \mu\text{C}/\text{m}^2$ along $[110]$ direction at 2 K²⁷. Moreover, an in-plane external magnetic field H can induce the rearrangement of the six multiferroic domains and every 60° rotation of the in-plane H leads to 120° flop of the P direction as a result of the flop of magnetic order.

Important questions concerning MnI_2 are why it has the helix spin magnetic ground state and how the spiral spin induces ferroelectric polarization. It is also of great interest in the appearance of successive phase transitions as temperature decreases. In this paper we perform a comprehensive theoretical investigation of these intriguing properties. We first calculate the magnetic exchange coupling parameters in MnI_2 and then discuss the magnetic phase transitions mentioned above within mean-field theory based on a Heisenberg-type magnetic exchange Hamiltonian, in which six exchange interactions are taken into account. And six exchange interactions are found to be necessary to give a good description of observed magnetic structure with Heisenberg model. We find that the inter-plane coupling is fairly strong because of its linear exchange path and is extremely important in inducing the spiral magnetic order ground state. We further calculate the polarization of MnI_2 and perform symmetry analysis to show the polarization is consistent with magnetic order. Finally, we show that the spin-orbit coupling (SOC) on I ions makes primary contribution to FE polarization, based on an analysis

of charge density difference between cases with and without SOC.

The paper is organized as following. First, in Sec. II, we perform DFT calculation to obtain the six exchange parameters from eight spin ordered arrangements and determine the magnetic modulation vectors of MnI_2 by using these exchange parameters. Then, in Sec. III, we determine the direction of the polarization in MnI_2 through symmetry analysis and calculate the polarization of different magnetic vectors using DFT. Finally, in Sec. IV, we give a summary and provide the main conclusions of our paper.

II. WAVE-VECTOR SELECTION IN MnI_2

A. Calculation of the exchange interaction parameters

Our DFT calculations employ the projector augmented wave (PAW) method encoded in Vienna *ab initio* simulation package (VASP)^{28–30}, and the generalized-gradient approximation (GGA) for the exchange correlation functional³¹ is used. Throughout this work, the cutoff energy of 400 eV is taken for expanding the wave functions into plane-wave basis. A set of $2 \times 4 \times 2$ Γ centered k-points is used for the $4 \times 2 \times 2$ supercell calculation, which is sufficient to obtain converged results for all quantities under consideration. It is well-known that GGA underestimates the correlation effect. To remedy this, the GGA plus on-site repulsion U method (GGA+U) in the formulation of Dudarev *et al.*³² is employed to describe the electron correlation effect associated with the Mn 3d states by an effective parameter U_{eff} .³³ Several U_{eff} values for Mn are taken in our calculations to check the validation of U_{eff} . In general, a proper choice of U_{eff} can systematically reproduce most of the experimental observations quite well. The self-consistent-field convergence is achieved when the total electronic energy difference between last two cycles is less than 10^{-7} eV. In all our calculations, we use the experimental crystal structure²⁴ as shown in Fig. 1. Mn ion is surrounded by octahedron of I ions and these octahedra are connected by sharing edges to form a triangle lattice of Mn atom in *ab* plane stacking along *c* lattice. Geometrically, it has inversion center and should have no electrical polarization. As discussed in the following, the noncollinear magnetic ordering breaks inversion symmetry and induces experimentally observed polarization, as well as the strong magneto-electric coupling effects.

In order to obtain the exchange parameters from DFT calculations, we separate the total energy into nonmagnetic (H_{non}) and magnetic contributions

$$H = H_{non} + \sum_{i < j} J_{ij} \hat{S}_i \cdot \hat{S}_j, \quad (1)$$

where \hat{S}_i and \hat{S}_j are the spin operators on sites *i* and *j*, respectively and the J_{ij} is the exchange interaction parameter between the sites *i* and *j*. $J_{ij} < 0$ corresponds to the ferromagnetic (FM) coupling between the two sites while $J_{ij} > 0$ corresponds to antiferromagnetic (AFM) interaction.

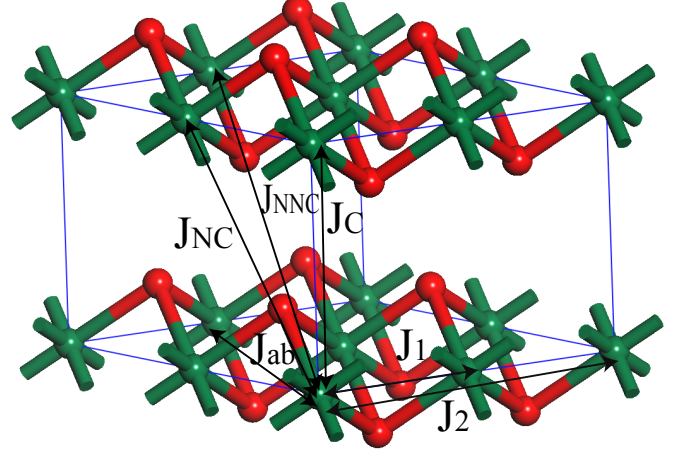


FIG. 1: (color online). Side view of the MnI_2 . The red and green atoms are Mn and I, respectively. The exchange parameters J_1 , J_{ab} , J_2 , J_C , J_{NC} and J_{NNC} between the cations connected by arrows are defined.

Fig. 1 illustrates the magnetic pair exchange interaction used in our modeling. J_1 , J_{ab} and J_2 are the intraplane interactions between the cations. J_C , J_{NC} and J_{NNC} are the interplane ones. As it can be seen from Fig. 1, the distance between Mn cations in the coupling J_{NNC} (9.910 Å) is much longer than that of the coupling J_C (6.829 Å) and J_{NC} (7.989 Å). One might expect that the coupling J_{NNC} is much weaker. However, according to Wollan *et al.*³⁴ J_{NNC} is fairly strong since it has an almost linear exchange path ($\text{Mn}^{2+} - \text{Br}^- - \text{Br}^- - \text{Mn}^{2+}$) in MnBr_2 , whose structure is isomorphous with that of MnI_2 . Our calculation shows that the magnitude of J_{NNC} is almost the same as J_C and J_{NC} , which confirms their conclusion.

The six spin exchange parameters can be evaluated by examining the eight ordered spin states of MnI_2 , i.e. the FM, AFM1, AFM2, AFM3, AFM4, AFM5, AFM6 and AFM7 states, defined in Fig. 2 in terms of a $4 \times 2 \times 2$ supercell. Table I summarizes the relative energies of these states per $4 \times 2 \times 2$ supercell, i.e. 16 f.u., determined from our GGA+U calculations with and without SOC included. From the energy expressions obtained for spin dimers with N unpaired spins per site (in present case, N=5)³⁵, the energies contributed by magnetic interactions in these eight magnetic states per f.u. can be written as

$$\begin{aligned} E_{FM} &= \frac{N^2}{4} (3J_1 + 3J_2 + 3J_{ab} + J_C + 6J_{NC} + 3J_{NNC}), \\ E_1 &= \frac{N^2}{4} (-J_1 + 3J_2 - J_{ab} + J_C - 2J_{NC} - J_{NNC}), \\ E_2 &= \frac{N^2}{4} (3J_1 + 3J_2 + 3J_{ab} - J_C - 6J_{NC} - 3J_{NNC}), \end{aligned}$$

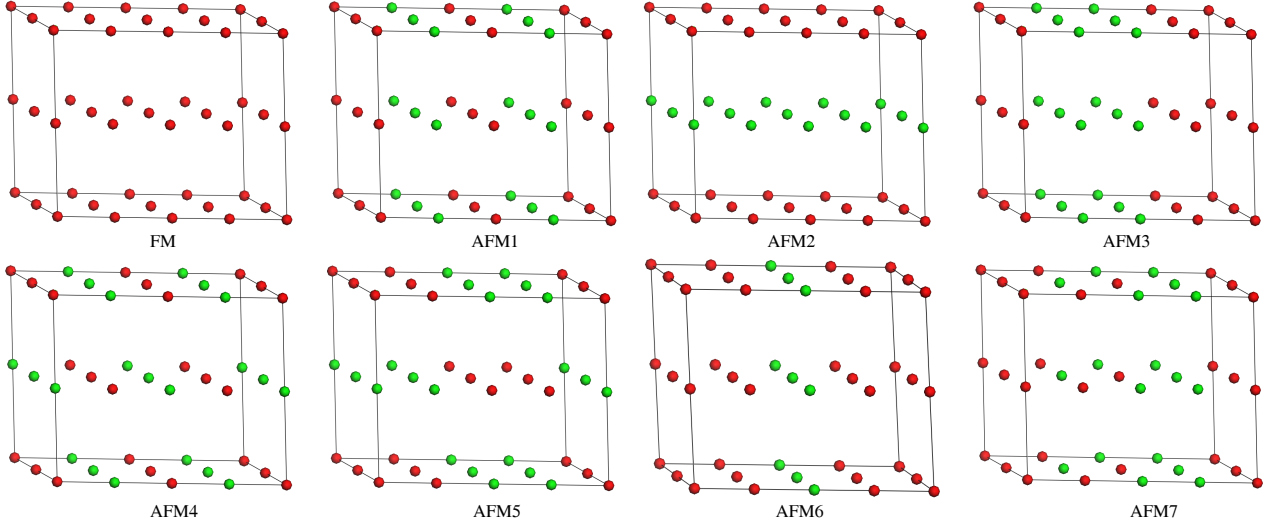


FIG. 2: (color online). Schematic plots of eight different magnetic ordering states of MnI_2 used for GGA+U calculation to extract the six spin-exchange parameters $J_1, J_2, J_{ab}, J_C, J_{NC}$ and J_{NNC} . The red and green circles represent the up and down magnetic moment on Mn sites, respectively.

$$\begin{aligned}
 E_3 &= \frac{N^2}{4}(J_1 - J_2 - J_{ab} + J_C + 2J_{NC} - J_{NNC}), \\
 E_4 &= \frac{N^2}{4}(-J_1 + 3J_2 - J_{ab} - J_C + 2J_{NC} + J_{NNC}), \\
 E_5 &= \frac{N^2}{4}(J_1 - J_2 - J_{ab} - J_C - 2J_{NC} + J_{NNC}), \\
 E_7 &= \frac{N^2}{4}\left(-\frac{1}{2}J_1 + J_2 - \frac{1}{2}J_{ab} + J_C - \frac{1}{2}J_{NC} + \frac{1}{2}J_{NNC}\right), \\
 E_6 &= \frac{N^2}{4}(J_1 + J_2 + J_C + 2J_{NC}). \tag{2}
 \end{aligned}$$

By mapping these onto the total energies obtained from DFT calculations, we obtain seven equations. But there are only six spin-exchange parameters, $J_1, J_{ab}, J_2, J_C, J_{NC}$ and J_{NNC} to be solved. For this overdetermined system of equations, we obtain these parameters by using a least-squares technique^{36,37}, and list them in Table II.

It is noted from the Table II that the intraplane exchange couplings J_1, J_2 and J_{ab} are antiferromagnetic for $U_{eff} \leq 3$ eV. However, J_1 becomes negative (i.e. to be ferromagnetic coupling) with $U_{eff} \geq 4$ eV, which is consistent with the estimated coupling in a similar compound MnBr_2 ³⁸ from neutron diffraction experiment. As a consequence, the intraplane spin-exchange interactions are geometrically frustrated. We notice that the exchange coupling is rather weak compared with similar compound such as CuCl_2 (exchange parameter is about 10 meV)³⁹. The weak exchange coupling can be expected from the observed low magnetic phase transition temperature (3.45K - 3.95K). The intraplane exchange coupling J_1 arises from two competing contributions, FM direct exchange and AFM superexchange interactions between two nearest Mns. The AFM superexchange interaction is mediated by two Mn-I-Mn bonds with the same bond angle 90.44° . For the similar case of Cu-O-Cu bonds, it has been shown that when the bond angle is close to 90° the resulting exchange energy is rather

small.⁴⁰ For the case of $U_{eff} = 4$ eV, one may notice that the coupling J_1 becomes ferromagnetic and weaker than J_2 in magnitude, although the distance of Mn-Mn in J_2 coupling is two times of that in J_1 . This seems strange but can be easily understood since both direct exchange and superexchange coupling contribute to J_1 . They have opposite signs and compete against each other. As U increases, the superexchange coupling becomes weaker while the direct exchange coupling is almost unchanged, which finally leads to a weak ferromagnetic coupling. J_1 becomes dominant for $U_{eff} = 5$ and 6 eV.

The interplane coupling parameters J_C, J_{NC} and J_{NNC} are AFM for all U_{eff} , which is consistent with the experiment carried out by Cable *et al.*^{24,25}. The fact that this two-anion indirect exchange coupling J_{NNC} appears to be antiferromagnetic might be expected by analogy with the single-anion superexchange mechanism. This coupling, which has linear exchange path ($\text{Mn}^{2+}-\text{I}^--\text{I}^--\text{Mn}^{2+}$), is stronger than the other two interplane couplings for $U_{eff} \leq 3$ eV. The magnitude of the three interplane interactions are almost the same for $U_{eff} = 4$ eV. J_{NC} and J_{NNC} become zero (< 0.01 meV) for $U_{eff} = 5$ and 6 eV.

From the theory of superexchange it follows that the corresponding coupling strength is proportional to $1/U$. If a coupling is mediated mainly by the superexchange interacting, one will expect a strong influence of the Hubbard parameter on the strength of this coupling. That is the reason why most of the exchange coupling strength decrease significantly with the increasing U_{eff} . The variation of J_{NNC} seems to show a $1/U$ dependence, as being mediated by superexchange interaction, which is consistent with the exchange path analysis above. While J_{ab} has less U_{eff} dependence, which is mainly a direct exchange coupling. We have further checked that SOC has little influence on exchange interactions, as shown for GGA and GGA+U ($U_{eff}=4.0$ eV) cases in Table II. Therefore, in the following we use the values obtained from the cal-

TABLE I: Relative energies (in meV) of eight ordered spin states of MnI₂ obtained from the GGA+U calculations with (yes) and without (no) SOC included for different U_{eff} values. In calculation with SOC, the spin quantization principle axis is in parallel with c axis.

| $U_{eff}(eV)$ | 0 | 0 | 1 | 2 | 3 | 4 | 4 | 5 | 6 |
|---------------|--------|--------|--------|-------|-------|-------|-------|-------|-------|
| SOC | no | yes | no | no | no | no | yes | no | no |
| FM | 0 | 0 | 0 | 0 | 0 | 0 | 0 | 0 | 0 |
| AFM1 | -258.7 | -250.2 | -149.5 | -81.1 | -35.8 | -4.8 | -2.8 | 16.8 | 32.1 |
| AFM2 | -83.1 | -82.9 | -58.4 | -41.5 | -29.6 | -21.0 | -21.0 | -14.7 | -10.1 |
| AFM3 | -203.8 | -199.3 | -127.9 | -79.0 | -45.8 | -22.7 | -21.6 | -6.3 | 5.4 |
| AFM4 | -241.8 | -233.2 | -137.7 | -73.1 | -30.6 | -1.7 | 0.3 | 18.5 | 32.7 |
| AFM5 | -210.7 | -206.4 | -133.2 | -83.4 | -49.8 | -26.3 | -25.3 | -9.6 | 2.4 |
| AFM6 | -166.6 | -162.3 | -101.3 | -59.7 | -31.9 | -12.6 | -11.5 | 1.1 | 10.8 |
| AFM7 | -253.6 | -245.6 | -150.4 | -85.3 | -41.9 | -12.0 | -10.2 | 9.0 | 23.9 |

TABLE II: Values of the spin-exchange parameters J (in meV) in MnI₂ obtained from the GGA+U calculations with (yes) and without (no) SOC included for different U_{eff} values. In calculation with SOC, the spin quantization principle axis is in parallel with c axis.

| $U_{eff}(eV)$ | 0 | 0 | 1 | 2 | 3 | 4 | 4 | 5 | 6 |
|---------------|------|------|------|------|------|-------|-------|-------|-------|
| SOC | no | yes | no | no | no | no | yes | no | no |
| J_1 | 0.49 | 0.46 | 0.27 | 0.13 | 0.03 | -0.03 | -0.03 | -0.07 | -0.10 |
| J_2 | 0.14 | 0.13 | 0.10 | 0.07 | 0.05 | 0.04 | 0.04 | 0.03 | 0.02 |
| J_{ab} | 0.03 | 0.03 | 0.02 | 0.01 | 0.01 | 0.01 | 0.01 | 0 | 0 |
| J_C | 0.04 | 0.04 | 0.03 | 0.02 | 0.02 | 0.01 | 0.01 | 0.01 | 0.01 |
| J_{NC} | 0.03 | 0.04 | 0.02 | 0.02 | 0.01 | 0.01 | 0.01 | 0 | 0 |
| J_{NNC} | 0.06 | 0.05 | 0.04 | 0.03 | 0.02 | 0.01 | 0.01 | 0 | 0 |

calculation without SOC.

B. The classical ground state of the MnI₂

To simplify the problem, we describe the magnetic ordering by a version of mean-field theory, in which one writes the magnetic free energy¹⁶ F_M as

$$H = \frac{1}{2} \sum_{\mathbf{r}_i, \alpha; \mathbf{r}_j, \beta} \chi_{\alpha\beta}^{-1}(\mathbf{r}_i, \mathbf{r}_j) S_\alpha(\mathbf{r}_i) S_\beta(\mathbf{r}_j) + O(S^4), \quad (3)$$

where $S_\alpha(\mathbf{r}_i)$ is the thermally averaged α component of the spin at position \mathbf{r}_i . Introducing Fourier transformations of $S_\alpha(\mathbf{r}_i)$ and $\chi_{\alpha\beta}^{-1}(\mathbf{r}_i, \mathbf{r}_j)$ and omitting high order terms, we have

$$F_M = \frac{1}{2} \sum_{\mathbf{q}; \tau_i, \tau_j, \alpha, \beta} \chi_{\alpha\beta}^{-1}(\mathbf{q}; \tau_i, \tau_j) S_\alpha(-\mathbf{q}; \tau_i) S_\beta(\mathbf{q}; \tau_j), \quad (4)$$

$$S_\alpha(\mathbf{q}, \tau_i) = \frac{1}{N} \sum_{\mathbf{R}} S_\alpha(\mathbf{R} + \tau_i) e^{i\mathbf{q} \cdot (\mathbf{R} + \tau_i)}, \quad (5)$$

$$\chi_{\alpha\beta}^{-1}(\mathbf{q}; \tau_i, \tau_j) = \sum_{\mathbf{R}} \chi_{\alpha\beta}^{-1}(\tau_i, \mathbf{R} + \tau_j) e^{i\mathbf{q} \cdot (\mathbf{R} + \tau_j - \tau_i)}, \quad (6)$$

where N is the number of the unit cells in the system, τ_i is the location of the i th site within the unit cell (τ_i is (0,0,0) in MnI₂), and \mathbf{R} is the lattice vector. As our main interest lies in explaining the observed magnetic modulation vector \mathbf{q} , we

have completely ignored anisotropy, whose major effect is to select the spin orientations. So we have an isotropic model,

$$\chi_{\alpha\beta}^{-1} = J_{\alpha\beta}(\tau_i, \tau_j) \delta_{\alpha\beta} + [K + dk_B T] \delta_{\alpha\beta} \delta_{\tau_i, \tau_j}, \quad (7)$$

where $\delta_{\alpha\beta}$ is unity if $\alpha = \beta$ and is zero otherwise. d is a spin-dependent constant of order unity, so that $-dk_B \sum_{\alpha} S_\alpha(\mathbf{r})^2$ is the entropy (relative to infinite temperature) associated with a spin S . In our case, we only consider the exchange couplings defined in Fig. 1. In our coordinate system, the lattice vectors are $\vec{a}_1 = a\vec{i}$, $\vec{a}_2 = -\frac{1}{2}a\vec{i} + \frac{\sqrt{3}}{2}a\vec{j}$ and $\vec{a}_3 = c\vec{k}$ (see Fig. 6, x1, y1), where a and c are the lattice constants of MnI₂. The reciprocal vectors are $\vec{b}_1 = \frac{2\pi}{a}(\vec{i} + \frac{\sqrt{3}}{3}\vec{j})$, $\vec{b}_2 = \frac{2\pi}{a} \cdot \frac{2\sqrt{3}}{3}\vec{j}$ and $\vec{b}_3 = \frac{2\pi}{c}\vec{k}$. Setting $\mathbf{q} = q_1\vec{b}_1 + q_2\vec{b}_2 + q_3\vec{b}_3$ in the Fourier transformation, we have the following $\chi^{-1}(\mathbf{q})$ with some algebra in MnI₂,

$$\begin{aligned} \chi^{-1}(\mathbf{q}) = & K + dk_B T \\ & + 2J_1[\cos(q_1) + \cos(q_1 + q_2) + \cos(q_2)] \\ & + 2J_{ab}[\cos(2q_1 + q_2) + \cos(q_1 + 2q_2) \\ & + \cos(-q_1 + q_2)] \\ & + 2J_2[\cos(2q_1) + \cos(2q_1 + 2q_2) + \cos(2q_2)] \\ & + 4J_{NC}[\cos(q_1) + \cos(q_1 + q_2) + \cos(q_2)] \cos(q_3) \\ & + 2J_C \cos(q_3) + 2J_{NNC}[\cos(q_1 + 2q_2 + q_3) \\ & + \cos(2q_1 + q_2 - q_3) + \cos(q_1 - q_2 + q_3)]. \quad (8) \end{aligned}$$

Setting $\chi^{-1}(\mathbf{q}) = K + dk_B T + J(\mathbf{q})$ and substituting the exchange parameters calculated with $U_{eff} = 4$ eV in Table II into Eq. (8), one can easily obtain the free energy surface in $\mathbf{q}(q_1, q_2, q_3)$ space. The minimum points of this

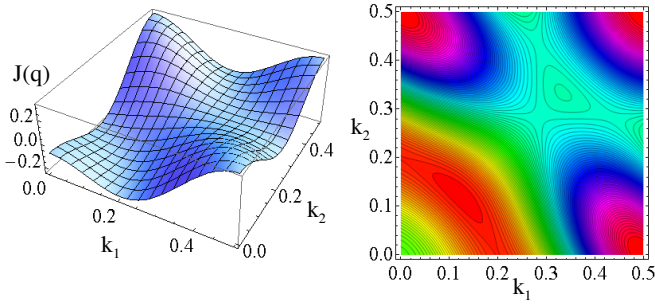


FIG. 3: (color online). The diagram of $\chi^{-1}(q_1, q_2, q_3)$ with q_3 fixed as experimental value 0.5 at T_{N1} . The minimum point is at $(q_1, q_2) = (0.1226, 0.1226)$, which is close to the experiment value $(0.1025, 0.1025)$.

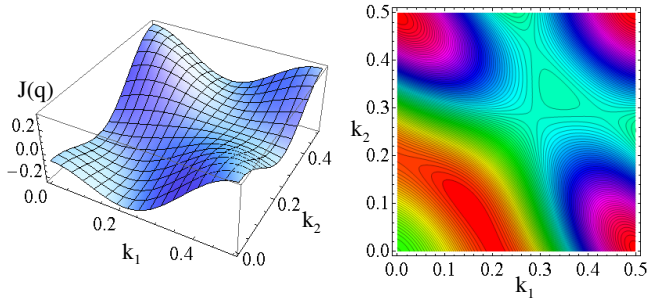


FIG. 4: (color online). The diagram of $\chi^{-1}(q_1, q_2, q_3)$ with q_3 fixed as experimental value 0.439 at T_{N3} . The minimum point is at $(q_1, q_2) = (0.155, 0.089)$, which is consistent with the experiment value $(0.181, 0)$.

surface might correspond to the experimentally determined magnetic modulation vectors at different temperature. In Fig. 3, by fixing $q_3=0.5$, the minimum point of χ^{-1} is at $(q_1, q_2) = (0.1226, 0.1226)$, which is in good agreement with experimental value $(0.1025, 0.1025)$ at transition temperature T_{N1} . By setting $q_3=0.439$, as shown in Fig. 4, we get $(q_1, q_2) = (0.155, 0.089)$ after minimizing χ^{-1} , which is also consistent with the experimental value $(0.181, 0)$ at T_{N3} . Assuming $q_2=0$ in the ground state, we minimize $\chi^{-1}(q_1, q_3)$ and obtain $(q_1, q_3) = (0.206, 0.444)$, which also reproduces the experimental values $(0.181, 0.439)$ at T_{N3} . Therefore, we believe $U_{eff}=4$ eV is proper for Mn in MnI_2 for the GGA+U calculation.

It is of interest to notice that \mathbf{q} vector has nonequivalent q_1 and q_2 when temperature is below T_{N3} , which means that $\chi^{-1}(\mathbf{q})$ should have asymmetric terms when exchanging q_1 and q_2 . The only possible term is that determined by J_{NNC} coupling with proper choice of q_3 . When the value q_3 is 0 or 0.5, $J(\mathbf{q})$ is invariant under the exchange of q_1 and q_2 . However, if q_3 is neither 0 nor 0.5, from Eq. 8 we find that the term contributed by J_{NNC} makes q_1 and q_2 inequivalent. Thus J_{NNC} is of crucial importance to the magnetic ground state, where q_1 is not equal to q_2 . Although the two layers of MnI_2 have a large separation about 3.5 Å, it cannot be treated as a quasi-2-D triangle lattice of Mn atoms due to the important interplane coupling J_{NNC} .

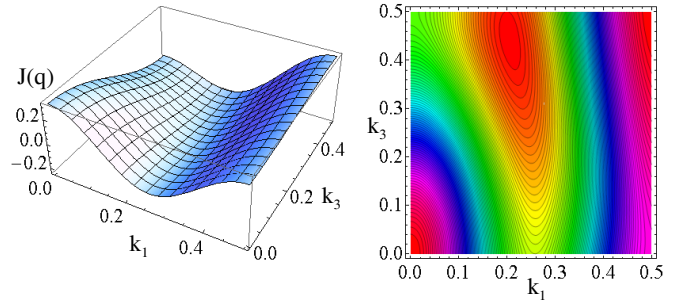


FIG. 5: (color online). The diagram of $\chi^{-1}(q_1, q_2, q_3)$ with q_2 fixed as experimental value 0 at T_{N3} . It is noted from above picture the minimum point is at $(q_1, q_3) = (0.206, 0.444)$, which is close to the experiment value $(0.181, 0.439)$.

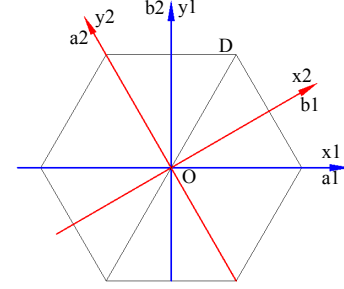


FIG. 6: (color online). The coordinate system in the paper. a_1 and a_2 denote the lattice basis while b_1 and b_2 denote the reciprocal basis.

In the mean-field approximation^{41,42}, the transition temperature T_N and Curie-Weiss temperature θ_{CW} are related to spin exchange parameters as

$$T_N = -\frac{S(S+1)}{3k_B} J(\mathbf{q})_{min}, \quad (9)$$

$$\theta_{CW} = -\frac{S(S+1)}{3k_B} \sum_i Z_i J_i, \quad (10)$$

where the sum is over all the nearest neighbors of a given spin site, Z_i is the number of the nearest neighbors connected by exchange coupling J_i , and S is the spin quantum number on each site (in present case $S = 5/2$). Therefore, the T_N and θ_{CW} are estimated to be 8.7 K and -10.7 K, respectively, using exchange parameters calculated from $U_{eff}=4$ eV, which is comparable with the experimental T_N 3.95 K and θ_{CW} -8 K⁴³. The ratio of the Curie-Weiss and the magnetic ordering temperature $\alpha \equiv |\theta_{CW}/T_{N1}|$ has been proposed as a quantitative measurement of frustration. In MnI_2 the ratio is about 2 in experiment, which is comparable with that of $\text{RbFe}(\text{MoO}_4)_2$ ($\alpha \sim 6$)⁴⁴ and is quite a low value with respect to NaTiO_2 ($\alpha > 500$)⁴⁵.

To end this section, we briefly give a summary. We obtain the exchange parameters through DFT calculation and use these parameters in Heisenberg exchange model to calculate the magnetic modulation vectors at different magnetic phase of MnI_2 . The intraplane couplings lead to frustration

TABLE III: General positions for $P\bar{3}m1$. Here "3" and "2" denote three fold and two fold rotation, respectively. m_n label the three mirror planes.

| | | |
|---|---|---|
| $E\mathbf{r} = (x, y, z)$ | $3\mathbf{r} = (\bar{y}, x + \bar{y}, z)$ | $3^2\mathbf{r} = (\bar{x} + y, \bar{x}, z)$ |
| $2_1\mathbf{r} = (y, x, \bar{z})$ | $2_2\mathbf{r} = (x + \bar{y}, \bar{y}, \bar{z})$ | $2_3\mathbf{r} = (\bar{x}, \bar{x} + y, \bar{z})$ |
| $I\mathbf{r} = (\bar{x}, \bar{y}, \bar{z})$ | $I3\mathbf{r} = (y, \bar{x} + y, \bar{z})$ | $I3^2\mathbf{r} = (x + \bar{y}, x, \bar{z})$ |
| $m_1\mathbf{r} = (\bar{y}, \bar{x}, z)$ | $m_2\mathbf{r} = (\bar{x} + y, y, z)$ | $m_3\mathbf{r} = (x, x + \bar{y}, z)$ |

in the triangle lattice of MnI_2 while the interplane coupling also has an important contribution. The nearest and next-nearest coupling compete with each other, which makes the spiral magnetism stable. The magnetic vectors obtained are in good agreement with those in experiment. The choice of U_{eff} is very important. In general, the criterion for choosing U value is to see whether it can well reproduce the experimental measurements systematically. In our case, we have checked that the calculated magnetic moment and the resulted magnetic modulation vectors, transition temperature, Currie-Weiss temperature, as well as the ferroelectric polarization are in good agreement with the experimental measurements when $U_{eff}=4.0$ eV. While other U_{eff} values (3, 5 and 6 eV) lead to large deviation or even qualitative error in some, or all of these physical quantities.

III. FERROELECTRICITY OF MnI_2

A. Symmetry analysis of MnI_2

In this section, we perform a group theoretical calculation for MnI_2 magnetic structure and determine the direction of the FE polarization. The ferroelectric polarization appears when temperature is below 3.45 K with a magnetic vector $\mathbf{q} \sim (0.181, 0, 0.439)^{27}$. The general positions of ions with space group $P\bar{3}m1$ are given in Table III.

Considering the wave vector $\mathbf{q} = q_x\hat{i} + q_z\hat{k}$ (in our second Cartesian coordinate x_2, y_2 , see Fig. 6), it is clear that the only operation (other than the identity) which conserves the wave vector is m_3 (mirror plane with respect to xz plane). We adopt the method in Ref. 16 to analyze the polarization of MnI_2 . Clearly, the Fourier component $S_x(\mathbf{q})$ obeys

$$\begin{aligned} m_3 S_x(\mathbf{q}) &= \lambda(m_3) S_x(\mathbf{q}), \\ m_3 S_z(\mathbf{q}) &= \lambda(m_3) S_z(\mathbf{q}), \end{aligned} \quad (11)$$

with $\lambda(m_3) = -1$, and that is irrep Γ_1 . For irrep Γ_2 , $\lambda(m_3) = 1$ and we have

$$m_3 S_y(\mathbf{q}) = \lambda(m_3) S_y(\mathbf{q}). \quad (12)$$

To fix the complex coefficients, we consider the effect of inversion, which leads to

$$IS_\alpha(\mathbf{q}) = S_\alpha^*(\mathbf{q}). \quad (13)$$

For Γ_1 , we consider its quadratic free energy and substitute Eq. (13), then $S_x(\mathbf{q})$ and $S_z(\mathbf{q})$ will have the same complex

phase.¹⁶ We now introduce order parameters which describe the magnitude and phase of these two symmetry labels (irreps). When both irreps are present, one has

$$\begin{aligned} S_x(\mathbf{q}) &= \sigma_1(\mathbf{q})r, \\ S_z(\mathbf{q}) &= \sigma_1(\mathbf{q})s, \\ S_y(\mathbf{q}) &= \sigma_2(\mathbf{q}), \end{aligned} \quad (14)$$

where $r^2 + s^2 = 1$ (r and s are real) and $\sigma_n(\pm\mathbf{q}) = \sigma_n e^{\mp i\phi_n}$. We also have the transformation properties

$$\begin{aligned} m_3\sigma_1 &= -\sigma_1, m_3\sigma_2 = \sigma_2, \\ I\sigma_1 &= \sigma_1^*, I\sigma_2 = \sigma_2^*. \end{aligned} \quad (15)$$

When both irreps are present, we have

$$\begin{aligned} S_x(\mathbf{r}) &= \sigma_1(\mathbf{q})r \cos(\vec{q} \cdot \vec{r} + \phi_1), \\ S_y(\mathbf{r}) &= \sigma_2(\mathbf{q}) \cos(\vec{q} \cdot \vec{r} + \phi_2), \\ S_z(\mathbf{r}) &= \sigma_1(\mathbf{q})s \cos(\vec{q} \cdot \vec{r} + \phi_1). \end{aligned} \quad (16)$$

Now we consider the magnetoelectric coupling in MnI_2 using order parameter obtained above. Since single order parameter cannot produce ferroelectricity in our case, we consider both irreps,

$$F_{int} = i \sum_{\gamma} r_{\gamma} P_{\gamma} [\sigma_1(\mathbf{q})\sigma_2^*(\mathbf{q}) - \sigma_1^*(\mathbf{q})\sigma_2(\mathbf{q})]. \quad (17)$$

Under operation m_3 , $\sigma_1(\mathbf{q})\sigma_2^*(\mathbf{q})$ and $\sigma_1^*(\mathbf{q})\sigma_2(\mathbf{q})$ will change sign. Since that F_{int} is invariant under m_3 , it requires P_{γ} to be odd under m_3 , so \vec{P} has to be along \hat{y} direction (y_2 direction in our second Cartesian coordinate), which is found in experiment²⁷.

B. Calculating the polarization using DFT

The electronic structure of MnI_2 calculated for FM state with $U_{eff} = 4$ eV is presented in Fig. 7. It is clear that FM state is insulating with an indirect band gap. Mn 3d states are mainly located in the lower energy region from -5.0 eV to -4.0 eV in the spin-up channel, and they are almost empty for the spin-down channel. Therefore, the Mn^{2+} ions in MnI_2 are high spin. The narrow and high peaks in density of states plot indicate that the 3d electrons of Mn are localized. The top of the valence band is primarily attributed to I 5p states, hybridized weakly with Mn 3d. The bottom of conduction band is mainly attributed to Mn 3d down spin states. The band dispersion is strong in ab plane but weak in c direction near fermi energy, as expected for the layered structure of MnI_2 .

As it has been shown that the propagation vector of MnI_2 is $\mathbf{q} = (0.181, 0, 0.439)$, we perform GGA+U with the experimental \mathbf{q} in absence of SOC, in which just one primitive cell is used due to the generalized Bloch theorem⁴⁶. Then we calculate the electric polarization using the Berry phase method⁴⁷. However, negligible polarization is found. The above observation leads us to consider SOC effect on the electric polarization in the spiral state of MnI_2 . We carry out GGA+U+SOC

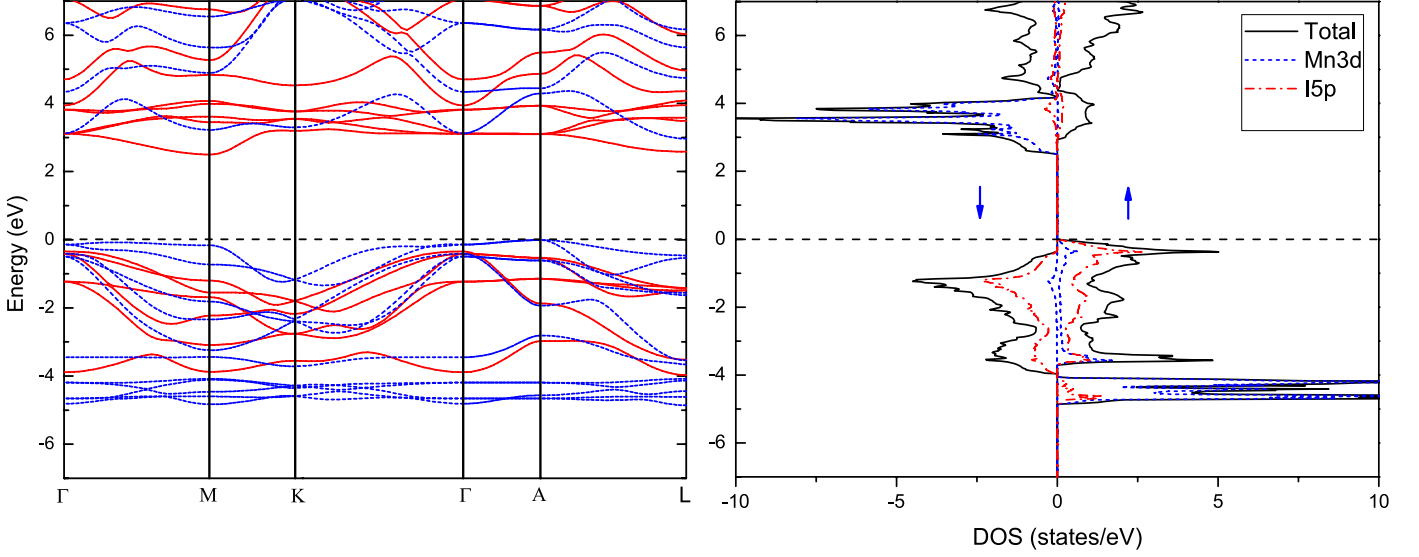


FIG. 7: (color online). Band structure and density of states(DOS) for MnI_2 calculated with GGA+U ($U_{eff}=4$ eV). Left panel is the band structure plot, the blue dash lines and red solid lines denote spin-up band and spin-down band, respectively. Γ is the center of the Brillouin zone , M (0,0.5,0), K($\frac{1}{3}, \frac{1}{3}, 0$), A (0,0,0.5) and L (0,0.5,0.5) in reciprocal lattice. Right panel is the DOS plot, the positive and negative value of DOS denote the majority spin states and the minority spin states, respectively.

($U_{eff} = 4$ eV) calculation for the $\mathbf{q} = (0.25, 0, 0.5)$ ⁴⁸ spiral states with spin in (307) plane²⁴. The polarization is $107.3 \mu\text{C}/\text{m}^2$ along a2 direction, which is consistent with polarization $\mathbf{P} \perp \mathbf{q}_{in}$ (0.25, 0, 0)²⁷. The experimental polarization is $84 \mu\text{C}/\text{m}^2$ at 2 K and the interpolated value at 0 K is about $128 \mu\text{C}/\text{m}^2$. The calculated polarization is a little bit smaller than the interpolated value, which is due to the approximation of the magnetic vector \mathbf{q} . As depicted in Ref. 27, the magnetic vector is parallel to [100] (in our coordinate is along OD, see Fig. 6), when high magnetic field along [100] is applied. In this case, we perform calculation with $\mathbf{q} = (\frac{1}{3}, \frac{1}{3}, 0)$ and the ferroelectric polarization is about $58 \mu\text{C}/\text{m}^2$ along OD, which is very close to $57 \mu\text{C}/\text{m}^2$ at $\theta_H = 30^\circ$ in high magnetic field²⁷ and consistent with experiment $\mathbf{P} \parallel \mathbf{q}_{in}$ ($\frac{1}{3}, \frac{1}{3}, 0$) but not with the prediction from KNB model¹⁷.

Obviously, the polarization of MnI_2 is induced by SOC, which is also consistent with the calculation of Xiang *et al.*⁴⁹. The spin-orbit part of Hamiltonian is $\hat{H}_{SO} = \lambda \hat{\mathbf{L}} \cdot \hat{\mathbf{S}}$, where λ is the spin-orbit coupling constant. SOC is expected to be strong on I 5p orbitals as the λ increases with the nuclear charge of the atom and decreases with increasing quantum numbers (angular quantum number and principle quantum number).

To examine how the polarization arises from the spiral magnetic state with SOC, we analyze the electron distribution of MnI_2 by showing the difference in electron density between calculations with and without SOC included for the case of $\mathbf{q} = (0.25, 0, 0.5)$. As shown in Fig. 8(a) that the main asymmetric charge distribution is around each I ion, which makes a primary contribution to the ferroelectric polarization. The graphical software XCrysDen⁵⁰ was used to plot

the electron density difference. The tremendous changes of charge density around I indicate that the SOC on I is rather strong. To study how spiral magnetism contributes to FE polarization, we analyze the electron distribution by showing the difference between the electron density of spiral state with $\mathbf{q} = (0.25, 0, 0.5)$ and that of FM state (a rather good reference state) of MnI_2 . Both calculations are performed with GGA+U+SOC. There is no FE polarization in FM state because the inversion symmetry is preserved, while it is broken by spiral magnetism, which is essential to appearance of FE polarization in MnI_2 . From Fig. 8(b), we find that there are changes of electron density around both Mn and I atoms. The strength of SOC on Mn is weaker compared with that of I, but it is also important. Spin-orbit interaction couples spin moment with electron's spacial orbital. As a result, the changes of spin direction will influence the spacial distribution of charge. The strong hybridization of Mn 3d and I 5p, as well as the strong SOC on I, will result in the asymmetric charge distribution around I atoms depending on the spin states of surrounding Mn atoms. That is why the electron density around I1 and I2(in Fig. 8(b)) looks different. Therefore, both spiral magnetism and SOC are essential to the FE polarization of MnI_2 . The spiral magnetism breaks the inversion symmetry and the degree of freedom of orbital couples with that of spin through SOC, which lead to asymmetric charge distribution (this is FE polarization). For the case of $\mathbf{q} = (\frac{1}{3}, \frac{1}{3}, 0)$, the electron density difference is similar to the case of $\mathbf{q} = (0.25, 0, 0.5)$. Furthermore, we find a linear relationship between the magnitude of electric polarization and the strength of SOC.

To examine the effect of ion displacement in the spin-spiral state on the FE polarization, we optimize the atoms positions

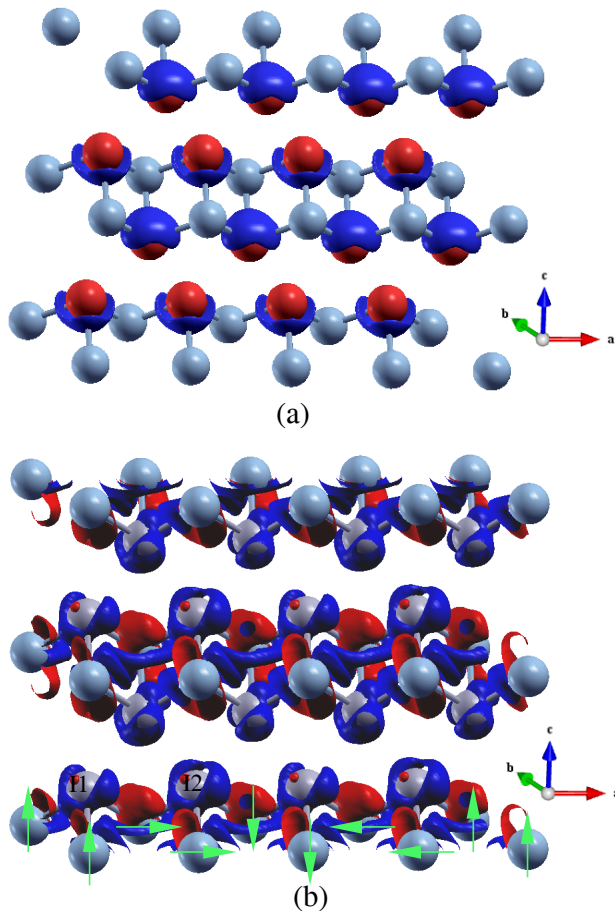


FIG. 8: (color online). (a) Perspective view of an isosurface calculated for the electron density difference between the GGA+U+SOC and GGA+U results for the case of $\mathbf{q}=(0.25, 0, 0.5)$. The red and blue surface represent $5.5 \times 10^{-4} e/\text{\AA}^3$ and $-5.5 \times 10^{-4} e/\text{\AA}^3$, respectively. (b) Perspective view of an isosurface calculated for the electron density difference between the spiral magnetic state ($\mathbf{q}=(0.25, 0, 0.5)$) and FM state with GGA+U+SOC. The red and blue surface represent $5.0 \times 10^{-5} e/\text{\AA}^3$ and $-5.0 \times 10^{-5} e/\text{\AA}^3$, respectively. The arrows on Mn atoms denote the direction of their spins. The electron distribution on I1 and I2 has visible difference.

of MnI_2 in the above two cases by performing GGA+U+SOC calculation until the atomic forces become less than $0.02 eV/\text{\AA}$ and then calculate the electric polarization using the relaxed structures. In the case of $\mathbf{q} = (0.25, 0, 0.5)$, it is found that Mn^{2+} ions move along a_2 direction, which leads to slightly enhanced FE polarization to about $170 \mu\text{C}/\text{m}^2$ in comparison with the value of $107.3 \mu\text{C}/\text{m}^2$ without ion displacement. For $\mathbf{q} = (\frac{1}{3}, \frac{1}{3}, 0)$, it is found that the sum of Mn displacements is along OD direction while that of I ions is along the opposite direction. The in-plane electric polar-

ization of the relaxed structure is greatly enhanced from $58 \mu\text{C}/\text{m}^2$ to $170 \mu\text{C}/\text{m}^2$ with direction of FE polarization reversed. The out-of-plane component in this case is about one third of the in-plane component.

IV. SUMMARY AND CONCLUSIONS

In this paper we have presented a comprehensive investigation of the incommensurate magnetic structure and ferroelectric polarization of the new multiferroic material MnI_2 . Six exchange interaction parameters among local moments on Mn sites are obtained by mapping the mean-filled Heisenberg model Hamiltonian onto the total energy differences of eight different magnetic ordering states from DFT calculations. We show the inter-plane coupling J_{NNC} is fairly strong because of its linear exchange path, as suggested before by Wollan *et al.*³⁴, although there is a large separation between the Mn-layers. As a result, the lattice of Mn cannot be simply treated as a quasi two dimensional system. Moreover, this inter-plane coupling J_{NNC} is critical to generating spiral spin structure by breaking the equivalence of the spin-density wavevectors along two different directions, q_1 and q_2 , in the magnetic ground state. Our calculation also indicates that Hubbard U_{eff} strongly affects the magnetic exchange couplings. It is found that $U_{eff} \sim 4 eV$ can give results quantitatively consistent with experimental values. For example, the Currier-Weiss temperature is estimated as $-10.7 K$ when $U_{eff} = 4 eV$, which is very close to $-8 K$ in the experimental measurement⁴³.

We also use both symmetry analysis and DFT calculations to investigate the polarization of this material. Our study reveals that SOC is essential for its ferroelectric polarization. Both the direction and magnitude of the polarization obtained from DFT calculation are in good agreement with the experimental data. Charge density difference analysis shows that the primary asymmetric charge distribution is around I ions, due to their strong SOC effect.

The isotropic Heisenberg model considered in this paper provides a good description of the magnetic ordering in MnI_2 . This suggests that the polarization induced by spiral magnetic ordering has no strong feedback effect on magnetic ordering. This result is consistent with the observed small value of polarization.

V. ACKNOWLEDGMENTS

We thank J.M. Zhang, J. Ding, Z. Liu and Y. R. Zhang for extremely useful discussion. The work is supported by "973" program (Grant No. 2010CB922904 and No. 2012CV821400), as well as national science foundation of China (Grant No. NSFC-1190024, 11175248 and 11104339).

* Electronic address: hmweng@iphy.ac.cn

† Electronic address: hfan@iphy.ac.cn

‡ Electronic address: jphu@iphy.ac.cn

¹ Y. Tokura, Science **321**, 1481 (2006).

² S.W. Cheong and M. Mostovoy, Nat. Mater. **6**, 13 (2007).

³ T. Kimura, T. Goto, H. Shintani, K. Ishizaka, T. Arima and Y.

- Tokura, Nature **426**, 55 (2003).
- ⁴ N. Hur, S. Park, P. A. Sharma, J. S. Ahn, S. Guha, and S.W. Cheong, Nature (London) **429**, 392 (2004).
 - ⁵ I. Kigomiya, S. Matsumoto, K. Kohn, Y. Fukuda, T. Shoubu, H. Kimura, Y. Noda, and N. Ikeda, Ferroelectrics **286**, 167 (2003).
 - ⁶ N. Hur, S. Park, P. A. Sharma, S. Guha, and S.W. Cheong, Phys. Rev. Lett. **93**, 107207 (2004).
 - ⁷ L. C. Chapon, G. R. Blake, M. J. Gutmann, S. Park, N. Hur, P.G. Radaelli, and S.W. Cheong, Phys. Rev. Lett. **93**, 177402 (2004).
 - ⁸ A. M. Kadomtseva, S. S. Krotov, Y. F. Popov, and G. P. Vorob'ev, Low Temp. Phys. **32**, 709 (2006).
 - ⁹ H. Katsura, A. V. Balatsky, and N. Nagaosa, Phys. Rev. Lett. **98**, 027203 (2007).
 - ¹⁰ L. C. Chapon, P. G. Radaelli, G. R. Blake, S. Park, and S.-W. Cheong, Phys. Rev. Lett. **96**, 097601 (2006).
 - ¹¹ Y. J. Choi, H. T. Yi, S. Lee, Q. Huang, V. Kiryukhin, and S.-W. Cheong, Phys. Rev. Lett. **100**, 047601 (2008).
 - ¹² T. Kimura, Annu. Rev. Mater. Res. **37**, 387 (2007).
 - ¹³ O. Auciello, J. F. Scott, and R. Ramesh, Phys. Today **51**, 22 (1998).
 - ¹⁴ N. A. Spaldin, S.-W. Cheong, and R. Ramesh, Phys. Today **63**, 38 (2010).
 - ¹⁵ M. Mostovoy, Phys. Rev. Lett. **96**, 067601 (2006).
 - ¹⁶ A. B. Harris, Phys. Rev. B **76**, 054447 (2007).
 - ¹⁷ H. Katsura, N. Nagaosa, and A.V. Balatsky, Phys. Rev. Lett. **95**, 057205 (2005).
 - ¹⁸ I. A. Sergienko and E. Dagotto, Phys. Rev. B **73**, 094434 (2006).
 - ¹⁹ A. B. Harris, J. Appl. Phys. **99**, 08E303 (2006).
 - ²⁰ J. P. Hu, Phys. Rev. Lett. **100**, 077202 (2008).
 - ²¹ C. Wang, G.-C. Guo, and L. He, Phys. Rev. Lett. **99**, 177202 (2007).
 - ²² S. Picozzi, K. Yamauchi, B. Sanyal, I. A. Sergienko, and E. Dagotto, Phys. Rev. Lett. **99**, 227201 (2007).
 - ²³ H. J. Xiang and M. H. Whangbo, Phys. Rev. Lett. **99**, 257203 (2007).
 - ²⁴ J. W. Cable, M. K. Wilkinson, E. O. Wollan and W. C. Koehler, Phys. Rev. **125**, 1860 (1962).
 - ²⁵ T. Sato, H. Kadowaki, K. Iio, Physica (Amsterdam) **213B-214B**, 224 (1995).
 - ²⁶ H.J.W.M. Hoekstra, P.R. Boudewijn, H. Groenier and C. Haas, Physica (Amsterdam) **121B +C**, 62 (1983); C.R. Ronda, H. H. Siekman and C. Haas, *ibid.* **144B+C**, 331 (1987).
 - ²⁷ T. Kurumaji, S. Seki, S. Ishiwata, H. Murakawa, Y. Tokunaga, Y. Kaneko and Y. Tokura, Rhys. Rev. Lett. **106**, 167206 (2011).
 - ²⁸ G. Kresse and J. Hafner, Phys. Rev. B **47**, 558 (1993).
 - ²⁹ G. Kresse and J. Furthmuller, Comput. Mater. Sci. **6**, 15 (1996).
 - ³⁰ G. Kresse and J. Furthmuller, Phys. Rev. B **54**, 11169 (1996).
 - ³¹ J. P. Perdew, K. Burke, and M. Ernzerhof, Phys. Rev. Lett. **77**, 3865 (1996).
 - ³² S. L. Dudarev, G. A. Botton, S. Y. Savrasov, C. J. Humphreys, and A. P. Sutton, Phys. Rev. B **57**, 1505 (1998).
 - ³³ A. I. Liechtenstein, V. I. Anisimov, and J. Zaanen, Phys. Rev. B **52**, R5467 (1995).
 - ³⁴ E. O. Wollan, W. C. Koehler and M. K. Wilkinson. Rhys. Rev. **110**, 638 (1958).
 - ³⁵ D. Dai and M.-H. Whangbo, J. Chem. Phys. **114**, 2887 (2001); **118**, 29 (2003).
 - ³⁶ G. Williams, Am. Math. Monthly **97**, 511 (1990).
 - ³⁷ H. Sims, S. J. Oset, W. H. Butler, J. M. MacLaren and M. Marsman, Phys. Rev. B **81**, 224436 (2010).
 - ³⁸ T. Sato, H. Kadowaki, H. Masuda and K Iio, J. Phys. Soc. Jpn. **51** 4583 (1994).
 - ³⁹ M. G. Banks, R. K. Kremer, C. Hoch, A. Simon, B. Ouladdiaf, J. M. Broto, H. Rakoto, C. Lee and M. H. Whangbo, Phys. Rev. B **80**, 024404 (2009).
 - ⁴⁰ S. Tornow, O. Entin-Wohlman, and A. Aharony. Phys. Rev. B **60**, 10206 (1999).
 - ⁴¹ J. S. Smart, *Effective Field Theory of Magnetism*, (Saunders: Philadelphia, 1966).
 - ⁴² T. Nagamiya, *Solid State Physics: Advances in Research and Applications*, edited by F. Seitz, D. Turnbull, and H. Ehrenreich (Academic, New York), Vol. 20, pp. 305-411 (1967).
 - ⁴³ H.J.W.M. Hoekstra, H. F. Folkersma and C. Haas, Solid State Commun. **51**, 657-661 (1984).
 - ⁴⁴ G. Gasparovic, Ph.D. thesis, Johns Hopkins University, 2004.
 - ⁴⁵ K. Hirakawa, and K. Ubukoshi, J. Phys. Soc. Japan **50** 1909 (1981).
 - ⁴⁶ L. M. Sandratskii, Adv. Phys. **47**, 91 (1988).
 - ⁴⁷ R. D. King-Smith and D. Vanderbilt, Phys. Rev. B **47**, 1651 (1993); R. Resta, Rev. Mod. Phys. **66**, 899 (1994).
 - ⁴⁸ Although the sign of the polarization from each layer MnI depends largely on its spin spiral chirality, we use $\mathbf{q} = (0.25, 0, 0.5)$ instead of $\mathbf{q} = (0.25, 0, 0)$ because the magnitude of FE polarization is in better agreement with that of the experiment.
 - ⁴⁹ H. J. Xiang, E. J. Kan, Y. Zhang, M. H. Whangbo and X. G. Gong, Rhys. Rev. Lett. **107**, 157202 (2011).
 - ⁵⁰ A. Kokalj, Comp. Mater. Sci. **28**, 155 (2003). Code available from <http://www.xcrysden.org/>